Transforming properties of a Q18→E mutation of the microtubule regulator Op18

David E. Misek,[1,4] Christina L. Chang,[1] Rork Kuick,[1] Robert Hinderer,[1] Thomas J. Giordano,[2] David G. Beer,[3] and Samir M. Hanash[1]

[1]Department of Pediatrics
[2]Department of Pathology
[3]Department of Surgery, University of Michigan, Ann Arbor, Michigan 48109
[4]Correspondence: dmisek@umich.edu

Summary

We have identified a somatic mutation in Op18 in a human esophageal adenocarcinoma. The mutant form of Op18 (M-Op18) was cloned and sequenced, revealing a substitution of a G for C at nucleotide 155, which results in a Q18→E substitution in the protein. M-Op18 cDNA was expressed in NIH/3T3 cells, which resulted in foci formation and tumor growth in immunodeficient mice. Cell cycle analysis of M-Op18-expressing cells revealed a doubling in the percentage of cells in G2/M relative to cells overexpressing wild-type Op18, a decrease in M-Op18-specific phosphorylation, and alterations in tubulin ultrastructure in M-Op18-expressing cells. These results suggest that the somatic mutation identified in Op18 has profound effects on cell homeostasis that may lead to tumorigenicity.

Introduction

Oncoprotein 18 (Op18) is an ubiquitous, highly conserved 19 kDa cytosolic protein that has been shown to destabilize microtubules in vitro, at least in part due to tubulin sequestration and microtubule catastrophe-promoting activities (Belmont and Mitchison, 1996; Horwitz et al., 1997; Jourdain et al., 1997; Larsson et al., 1997). Op18 is expressed in proliferating cells of most cell lineages (Rowlands et al., 1995), and its level increases significantly during the S phase of the cell cycle (Cooper et al., 1989; Strahler et al., 1992a). The functionality of Op18 is also tightly controlled by phosphorylation during the cell cycle (Strahler et al., 1992a), with its activity being downregulated by increased phosphorylation on four serine (S16, S25, S38, and S63) residues (Gavet et al., 1998; Horwitz et al., 1997). Higher-order phosphorylation is a prerequisite for progression through mitosis. Mono- and biphosphorylated Op18 isoforms are most abundant in cells during the S phase, and the triphosphorylated Op18 isoform is predominant in G2/M (Beretta et al., 1993; Larsson et al., 1995; Strahler et al., 1992b). In vitro, S25 and S38 are targets of MAP kinases. Cyclin-dependent kinases phosphorylate Op18 on S25 and S38 (Beretta et al., 1993; Marklund et al., 1993). S16 is the target for the Ca^{2+}/calmodulin-dependent kinases II and IV/Gr (Marklund et al., 1994). S63 and S16 are substrates for cAMP-dependent protein kinases (Beretta et al., 1993; Curmi et al., 1994). Being a substrate of several kinase families, Op18 has been proposed to act as a relay phosphoprotein for multiple signal transduction pathways (Sobel, 1991).

The importance of Op18 phosphorylation in cell cycle progression was demonstrated by using transfectants expressing a phosphorylation site-deficient mutant form of Op18 (in which the four phosphorylatable serine residues were replaced with alanines (4A mutant). Overexpression of this mutant prevented formation of a normal mitotic spindle and led to a G2/M arrest and subsequent polyploidization (Gavet et al., 1998; Marklund et al., 1996). The 4A nonphosphorylatable mutant simulates the active form of Op18, suggesting that downregulation of Op18-mediated microtubule-destabilizing activity is required for spindle formation and mitotic progression. Although overexpression of wild-type phosphorylatable Op18 destabilized interphase microtubules, it did allow for proper spindle formation and normal progression through the cell cycle (Gavet et al., 1998; Marklund et al., 1996). The involvement of Op18 in spindle formation appears to function through an interaction with tubulin dimers that regulate microtubule dynamics (Belmont and Mitchison, 1996).

Given its role as an important regulator in proliferation and differentiation, deregulated expression of Op18 may be relevant to cancer. An increased level of Op18 expression has been

SIGNIFICANCE

Although microtubules have been extensively studied as targets of cancer therapeutics (e.g., Taxol, vindesine, and vincristine), only truncation mutations of the Adenomatous polyposis coli protein have been implicated in human neoplasia. The microtubule-regulating protein Op18 has been shown to destabilize microtubules in vitro, at least in part due to tubulin sequestration and microtubule catastrophe-promoting activities. In this report, we have identified a somatic mutation in Op18 in a human esophageal adenocarcinoma. Functional analyses have demonstrated that expression of the mutant Op18 in NIH/3T3 cells induces transformation in vitro and tumor development in nude mice. We have described a novel mutation in a microtubule-regulating protein, suggesting that regulation of microtubule dynamics may have a causal relationship to human neoplasm.

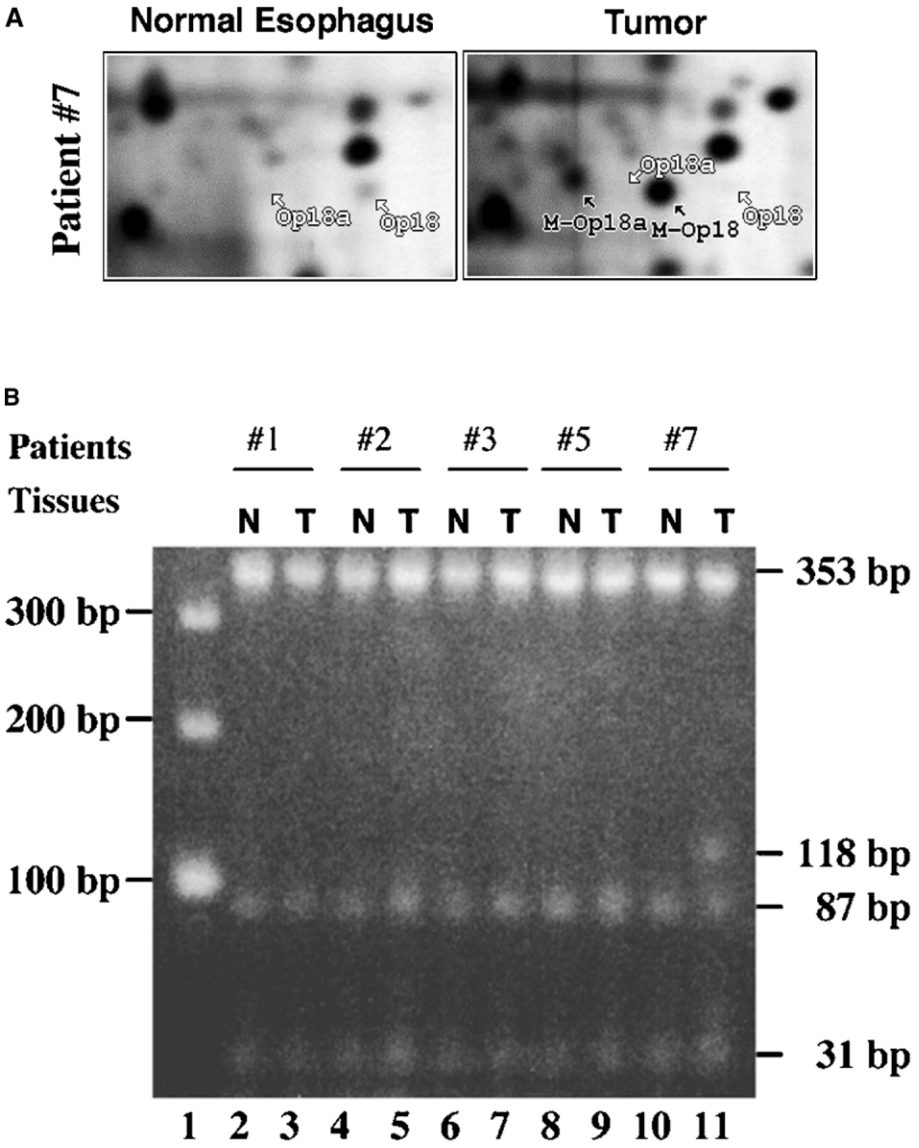

Figure 1. Identification of a somatic mutation in Op18 in a human esophageal adenocarcinoma

A: 2D PAGE analysis of Op18 isoforms in normal and tumor tissues. Proteins from solubilized tissues obtained from Patient #7 were separated by 2D PAGE, followed by silver staining, as described in Experimental Procedures. Only the close-up sections framing Op18 protein isoforms from normal esophageal tissue and the patient's tumor are shown. Op18 isoforms were identified based on their characteristic location in 2D patterns and based on their reactivity with an anti-Op18 antibody. Arrows point to unphosphorylated form of Op18 (Op18) and a major phosphorylated isoform (Op18a). Novel proteins are indicated as M-Op18 and M-Op18a. **B**: Detection of C_{155}→G mutation in the Op18 gene. Genomic DNA was isolated from five esophageal tumors and the corresponding normal gastric mucosa, and the mRNA encoding Op18 was amplified by PCR. The PCR products were digested with ScrF1 restriction enzyme and subsequently analyzed by gel electrophoresis, as described in Experimental Procedures. Lane 1: M.W. markers. Lanes with even numbers contain PCR products amplified from normal esophageal tissue, whereas those with odd numbers contain PCR products amplified from esophageal tumors. ScrF1 digestion of the 489 bp PCR products amplified from wild-type Op18 gene would generate 353, 87, 31, and 17 bp fragments. The C_{155}→G mutation in the Op18 gene eliminates a ScrF1 site between the 87 bp and 31 bp fragments, resulting in a 118 bp fragment, which was only observed in the tumor but not the normal esophageal tissue of patient #7 (lane 11 versus 10). In lane 11, the 87 bp fragment was also detected, displaying a similar intensity as the 118 bp fragment. This is likely to be due to contaminating cell types in the tumor.

reported in acute leukemia (Hanash et al., 1988; Roos et al., 1993), lymphoma (Brattsand et al., 1993; Roos et al., 1993), neuroblastoma (Hailat et al., 1990), and breast carcinoma (Curmi et al., 2000). In this study, we have identified a somatic Q18→E mutation in Op18 in an esophageal adenocarcinoma. Functional analyses of this mutation demonstrated that the mutant Op18 has transforming properties.

Results

A point mutation detected in the Op18 coding region

As part of a proteomic analysis of esophageal adenocarcinomas, two-dimensional polyacrylamide gel electrophoresis (2D PAGE) was undertaken for 17 tumors and their corresponding normal and dysplastic (Barrett's) tissue. Interestingly, one tumor showed a total lack of the major Op18 isoform by 2D PAGE, as well as the appearance of a novel neighboring protein spot. The novel protein was absent in normal and dysplastic esophageal tissue from the same patient (Figure 1A) and was not present in the normal, dysplastic, or tumor tissues of the other 16 patients analyzed (data not shown). The novel protein displayed a similar molecular mass as Op18 but with a more acidic isoelectric point, suggesting that it may either be a variant of Op18 or an unrelated protein. Using an anti-Op18 polyclonal antibody, we examined whether this protein was an Op18 variant by 2D PAGE and Western blot analysis. Interestingly, the anti-Op18 antibody recognized this novel protein (not shown), thereby indicating a potential somatic mutation(s) in Op18.

PolyA$^+$ RNA was isolated from the tumor and subjected to RT-PCR to amplify the Op18 cDNA. The PCR products were purified and used directly for DNA sequencing analysis to avoid random mutations that might be introduced by *Taq* polymerase. A substitution of a G for C was detected at nucleotide 155 in the Op18 cDNA.

The C_{155}→G substitution in Op18 cDNA results in an elimination of a ScrFI restriction site, providing a basis for developing a PCR/restriction method to screen for this mutation in genomic DNA. Genomic DNA was isolated from normal and tumor tissues

of the 17 patients. Sequences in exon 3 and intron 4 of the Op18 gene (Melhem et al., 1991) were selected for primer design to amplify the 489 bp fragment. Subsequently, the PCR products were cut with ScrFI enzyme that generated four fragments (353 bp, 87 bp, 31 bp, and 17 bp) from the wild-type Op18 gene (Figure 1B). An elimination of a ScrFI site caused by the C_{52}→G mutation in the Op18 coding region would not generate the 87 bp and 31 bp fragments but instead would create a 118 bp fragment. We observed a 118 bp fragment in the tumor with the novel Op18 protein (Figure 1B). An additional 87 bp DNA fragment was also detected that displayed similar band intensity as the 118 bp fragment.

The C_{155}→G mutation in the Op18 cDNA results in a substitution of a glutamic acid for a glutamine at residue 18 of the protein. Using the Wisconsin Package (Genetics Computer Group, Inc.), the calculated pI values for the wild-type and mutated Op18 are 5.87 and 5.60, respectively. The acidic shift of pI caused by C_{52}→G mutation in Op18 is consistent with the observed pI value of the novel protein on the 2D gel (Figure 1A).

Generation of infectants that expressed the mutated Op18 (M-Op18)

To further investigate the biological significance of the Q18→E mutation in Op18, the wild-type (S-Op18), mutant Op18 (M-Op18), and antisense (AS-Op18) cDNA were subcloned into the pTP2000 bicistronic expression vector and transfected into the ϕNX retrovirus-producing cell line. The resulting retrovirus was used to infect the NIH/3T3 cell line and allowed to integrate into the cell genome. Stable transfectants remained as pooled populations of cells so as not to bias the results due to potential insertional inactivation of genes important for cell proliferation and differentiation. Expression of wild-type (S-Op18), antisense (AS-Op18), and the mutant form of Op18 (M-Op18) were coupled to neomycin resistance in the pTP2000 retroviral vector and were under the control of a CMV promoter. The expression of each infectant was found to be maximal in the presence of 400 μg/ml G418 (data not shown). The level of endogenous wild-type Op18 expressed in the M-Op18 infectants was ~1.5-fold higher than M-Op18 (data not shown), and the total amount of Op18 expressed in M-Op18 was comparable to that found in S-Op18. The level of wild-type Op18 in the M-Op18 infectants was similar to that found in the vector-only NIH/3T3 cell infectants (data not shown), a negative control infected only with retrovirus produced from the pTP2000 construct. In order to demonstrate that the expressed mutant gene was indeed a mutated form of Op18, M-Op18 and S-Op18 cell lysates were resolved by 2D gel electrophoresis. The resolved proteins were transferred onto PVDF membranes and subjected to antibody hybridization with specific rabbit anti-Op18 antibodies, followed by chemiluminescent visualization of the bound antibody (Figure 2A). Wild-type isoforms of Op18 were visualized on blots prepared from both cell lysates. Additionally, spots of reactivity appeared on the M-Op18 blots that colocalized with the spots attributed to expression of the mutant Op18. Thus, the M-Op18 NIH/3T3 cells did express a mutant form of Op18, and this mutated form of Op18 had an equivalent shift in the pI to that seen in the tumor from patient #7. Pulse-chase experiments (data not shown) demonstrated that the half-life of M-Op18 protein was similar to that of wild-type Op18 (approximately 8 hr in both M-Op18 and S-Op18 clones). This indicates that Q18→E mutation in Op18 did not affect its protein stability.

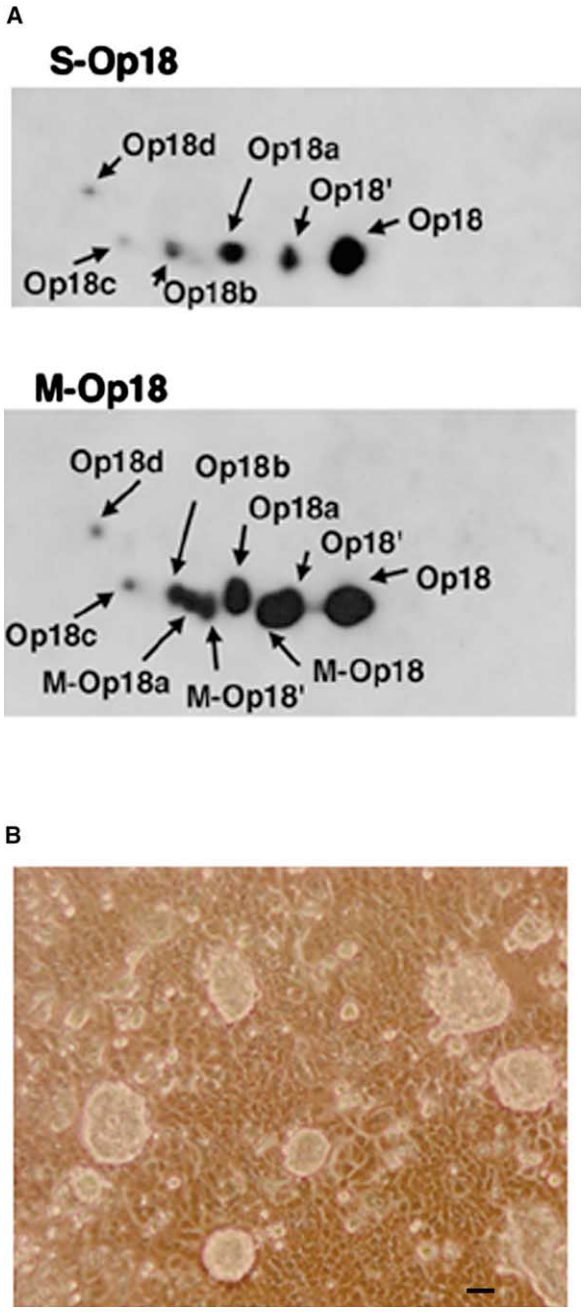

Figure 2. Expression of M-Op18 in NIH/3T3 cells

A: M-Op18 and S-Op18 isoforms are expressed in NIH/3T3 infectants. Proteins from solubilized NIH/3T3 infectants were separated by 2D PAGE, as described in Experimental Procedures, and subjected to Western blot analysis. Only the close-up sections framing Op18 protein are shown. Arrows point to unphosphorylated forms of Op18 (labeled Op18 and Op18′, respectively), a major isoform (Op18a), which is phosphorylated on one of the four phosphorylatable serine residues, and several minor isoforms, which are phosphorylated on several serine residues (Op18b, c, and d, respectively). The unphosphorylated mutant form of Op18 is indicated as M-Op18, and its major phosphorylated (on a single serine residue) isoform is indicated as M-Op18a. Interestingly, minor isoforms of M-Op18 that were phosphorylated on several serine residues were not observed. **B**: M-Op18 infectants form foci when grown in culture. M-Op18 infectants were propagated in culture for up to 1 week, as described in Experimental Procedures. The cells were photographed on an inverted microscope. Bar equals 50 μm.

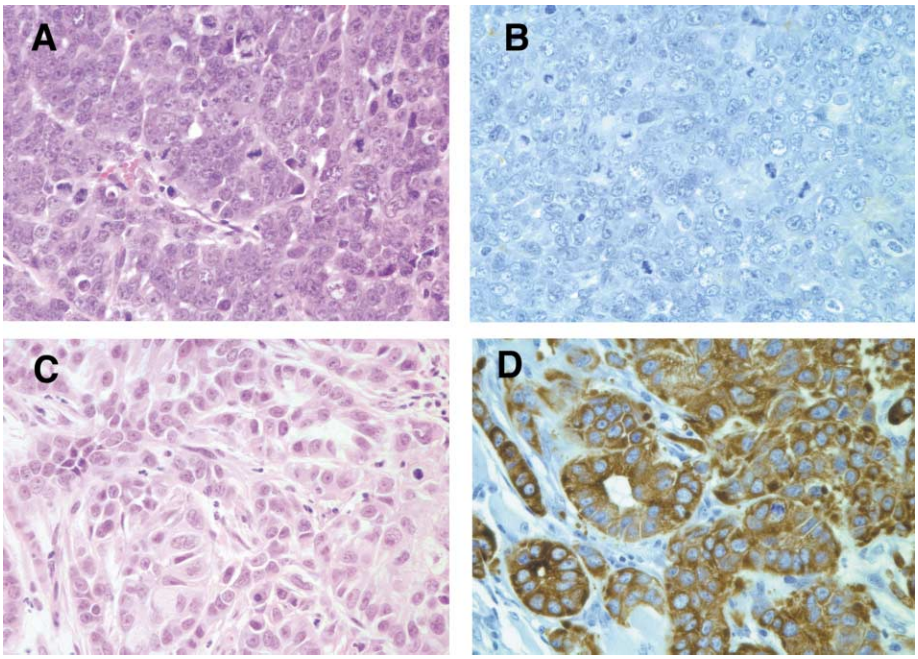

Figure 3. Histology and immunohistochemistry of tumors formed by subcutaneous inoculation of M-Op18 into immunodeficient mice

Tumors formed subsequent to M-Op18 inoculation into immunodeficient mice were harvested, trimmed of adipose and connective tissue, and then fixed in 10% buffered formalin. The tumors were embedded in paraffin, sectioned, and stained with Hematoxylin and Eosin (**A** and **C**) or for immunohistochemistry using a cytokeratin antibody (AE1/AE3) cocktail (**B** and **D**). The four images shown are from the same tumor, with **A** and **B** showing areas of high-grade neoplasm, and **C** and **D** showing areas of high-grade adenocarcinoma.

Moreover, the mutated Op18 did not appear to affect either the level of expression or the protein stability of wild-type Op18 in M-OP18 transfectants.

Transforming properties of M-Op18 (Q18→E)

The stably infected cell cultures were maintained in plastic culture flasks under G418 selection. Upon reaching confluence, the M-Op18 infectants were observed to form large numbers of foci, consisting of up to approximately 100 cells (Figure 2B). These foci have been observed in cells cultured (without passage) for up to 2 months. Foci formation was not observed with S-Op18, nor with infectants expressing antisense of Op18 (AS-Op18) and vector-only controls, indicating that the specific expression of M-Op18 in NIH/3T3 cells leads to foci formation.

We ascertained the ability of both the M-Op18 and S-Op18 cell populations to grow in an anchorage-independent fashion, a hallmark of the tumorigenic state. 1×10^4 cells of each infectant was plated in 0.35% Noble agar over a cushion of 0.7% Noble agar, in quintuplicate. Cells were fed full-growth medium (90% DMEM, 10% FCS containing antibiotics and G418 [400 μg/ml]) and assayed for growth at 35 days using an inverted microscope. We observed efficient colony formation in soft agar only with cells expressing M-Op18. M-Op18 infectants exhibited an average of 32.3 colonies (standard deviation = 14.3 colonies) per plate, compared to an average of 2.5 colonies (SD = 1.9 colonies) for S-Op18, an average of 2.3 colonies (SD = 0.6 colonies) for AS-Op18, and an average of 8.7 colonies (SD = 0.6 colonies) for vector only. We next determined the ability of cells expressing M-Op18 to form tumors in SCID mice. 5×10^6 cells (either M-Op18 or S-Op18) were inoculated subcutaneously into immunodeficient SCID C.B-17 mice in the intrascapular region. Tumors greater than 5 mm in diameter (range = 5–7 mm) were observed within 21 days in 10/10 mice inoculated with M-Op18. No tumors were observed in the ten mice inoculated with S-Op18 cells. The tumors were harvested under sterile

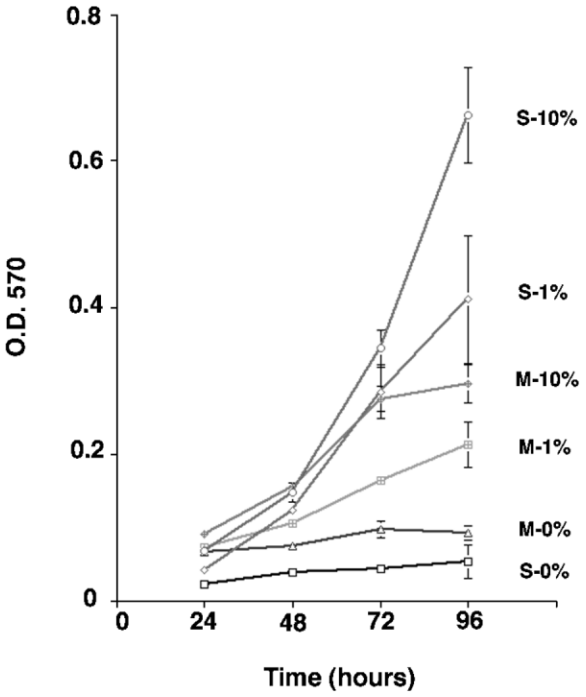

Figure 4. S-Op18 and M-Op18 infectants exhibit differences in growth rates when propagated in reduced serum levels

Serum-dependent growth was compared between the M-Op18 and S-Op18 cells. 5.0×10^3 cells of M-Op18 and S-Op18 were cultured in 96-well plates at 10%, 1%, or 0% serum concentration for up to 96 hr. Cell growth was determined by the MTT assay. The experiment has been repeated twice.

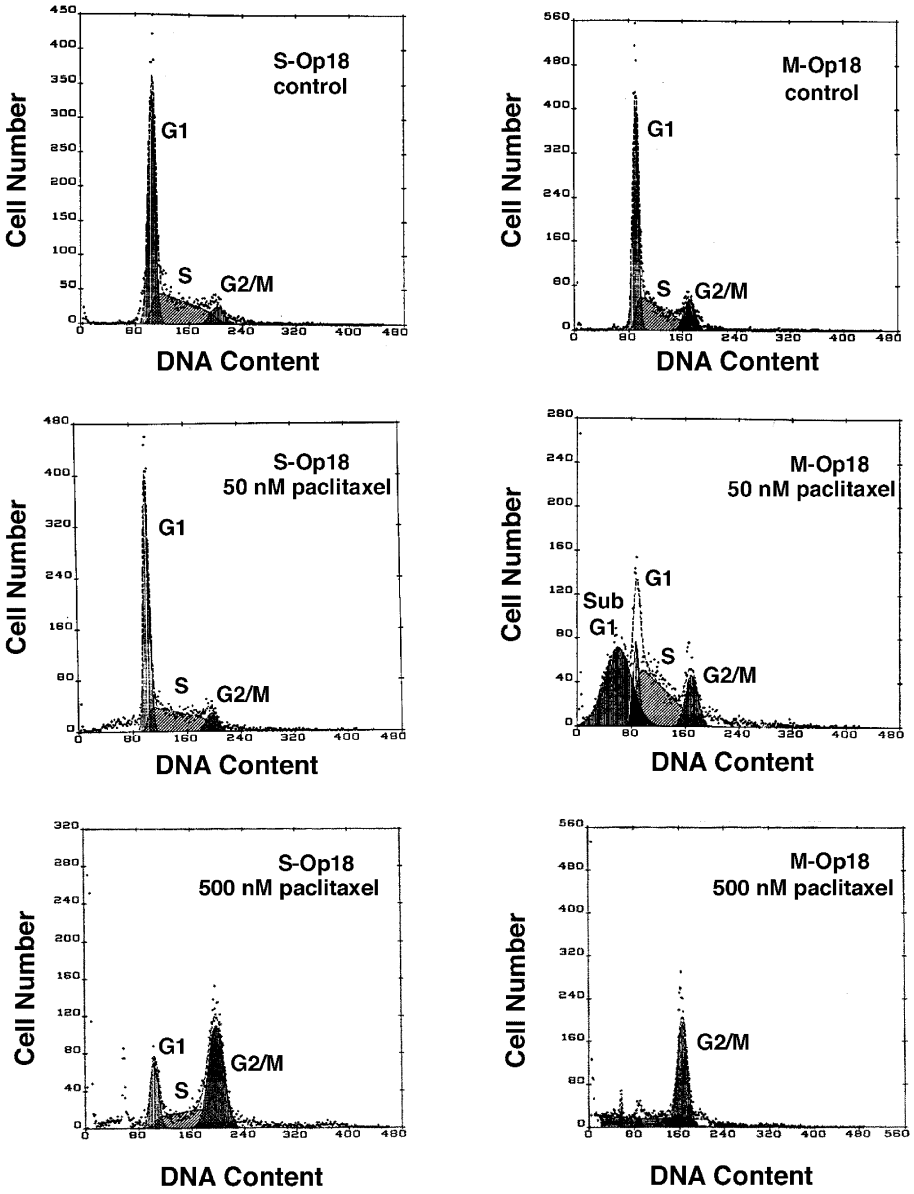

Figure 5. Cell cycle distribution of M-Op18 and S-Op18 infectants

M-Op18 and S-Op18 infectants were plated and grown at subconfluent levels for 48 hr and then treated minus and plus Paclitaxel for an additional 24 hr, as described in Experimental Procedures. Treatment groups were analyzed by flow cytometry for cell cycle distribution at 72 hr following plating. Cell cycle distribution of S-Op18 control (absence of Paclitaxel) and in the presence of 50 nM Paclitaxel and 500 nM Paclitaxel is shown, as is cell cycle distribution of M-Op18 control (absence of Paclitaxel) and in the presence of 50 nM and 500 nM Paclitaxel.

conditions and cell lysates were prepared from each tumor. Protein expression in the tumor nodules was analyzed by 2D PAGE. These tumors were found to maintain expression of M-Op18 (data not shown). Pathologically, these infected NIH/3T3 cells expressing M-Op18 formed malignant tumor nodules with biphasic morphology (Figure 3), appearing as high-grade neoplasms with areas of high-grade adenocarcinoma. The epithelial nature of the adenocarcinoma was evidenced by glandular formation and confirmed by expression of cytokeratins (Figure 3), whereas the component that was cytokeratin negative likely represents an undifferentiated neoplasm.

Effects of M-Op18 (Q18→E) on cell growth

To determine if the Q18→E mutation in Op18 affects growth properties, cells were grown at an initial density of 5×10^4 cells/ml for up to 4 days, and the growth rate of M-Op18 was compared to S-Op18, AS-Op18, and vector-only controls. Interestingly, although the Q18→E mutation had transforming properties, M-Op18 infectants exhibited a doubling time of 34.4 hr (±1.9 hr), compared to a doubling time of 23.1 hr (±2.3 hr) for S-Op18, a doubling time of 24.3 hr (±2.4 hr) for AS-Op18, and a doubling time of 21.6 hr (±2.1 hr) for vector only.

Serum-dependent growth was also compared between the M-Op18 and S-Op18 cells. At an initial density of ~5.0×10^3 cells/well of a 96-well plate, M-Op18 and S-Op18 were cultured at 10%, 1%, and 0% serum concentration for up to 96 hr. A slower growth rate was observed for both M-Op18 and S-Op18 when the serum level was reduced during culture (Figure 4). At the 10% serum level, M-Op18 exhibited a lower cell density, which apparently was reflected by its reduced growth rate relative to S-Op18. When the serum level was reduced to 1%, M-Op18 cells displayed a much lower density relative to S-Op18 cells. The results indicate that expression of the mutated form of Op18 affected serum-dependent growth. Thus, although ex-

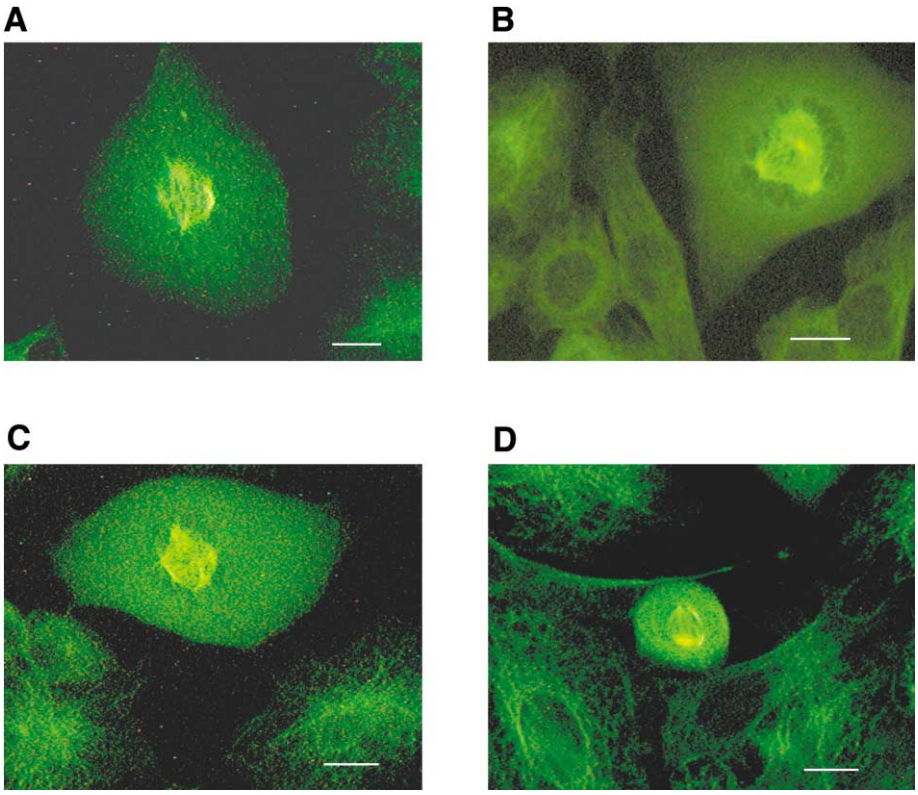

Figure 6. M-Op18 expression results in multipolar spindle formation in NIH/3T3 infectants

M-Op18 infectants were plated and grown at subconfluent levels for 48 hr and then fixed and stained for immunofluorescence with mouse anti-α-tubulin antibodies as described in Experimental Procedures. Mitotic spindles were observed and classified as being either normal (e.g., two poles) or multipolar (e.g., more than two poles). Three examples of multipolar spindles stained with the anti-α-tubulin antibody (**A–C**) are shown, as is an example of a normal bipolar spindle from S-Op18 infectants (**D**). The experiment has been repeated three times. Bar equals 10 μm.

pression of M-Op18 leads to cell growth retardation of a bulk population of cells, the mutant exerts transforming properties.

Effect of M-Op18 on microtubules

As the cell doubling time of the M-Op18 infectants was reduced relative to sense and vector-only infectants, we determined the effect of M-Op18 on cell cycle distribution and on microtubules. Additionally, as the unphosphorylated form of Op18 has been shown to bind and stabilize microtubules in vivo, we explored whether addition of various concentrations of Paclitaxel (which in sufficient concentration will itself cause a G2/M blockage of the cell cycle) would further perturb cell cycle progression of M-Op18 as compared with S-Op18. Both the M-Op18 and S-Op18 stably infected cell populations were plated at subconfluent levels in 10% serum for 48 hr, then treated with increasing concentrations of Paclitaxel for an additional 24 hr. All treatment groups were analyzed by flow cytometry for cell cycle distribution at 72 hr following plating (Figure 5). The percentages of M-Op18-expressing cells at each stage of the cell cycle were compared with those observed with the S-Op18 cell phenotype. In the absence of Paclitaxel, we observed a doubling of the percentage of M-Op18 cells in G2/M as compared to S-Op18, indicating that the retardation of doubling times observed in the M-Op18 cell population most likely resulted from a G2/M cell cycle stage-specific blockage. Intermediate concentrations of Paclitaxel (50–100 nM), which do not cause a complete G2/M block in the cell cycle, caused the appearance of a novel sub-G1 peak in M-Op18, consisting of 35.9%–45.8% of the total cell population, which was not observed in S-Op18 under similar conditions. The novel peak is indicative of a cell population that contains less genomic DNA than that which appears in the G1 population, and which could result from either apoptosis or segregation of chromosomes to multipolar (more than two) spindles, during mitosis. Thus, we examined the two cell populations for levels of apoptosis but were unable to discern any differences (data not shown). Moreover, incubation in as little as 100 nM Paclitaxel for 24 hr resulted in a significantly increased percentage of M-Op18 cells in G2/M (42% M-Op18 as compared with just 9% S-Op18). Incubation in 500 nM Paclitaxel resulted in an almost complete arrest in G2/M for M-Op18 (95.7%), whereas S-Op18 exhibited 53.9% of the cell population in G2/M. Both cell lines exhibited a complete G2/M arrest at the highest Paclitaxel concentration tested (1 μM). Taken together, these results suggest that expression of the mutated form of Op18 may enhance stability of microtubules through the cell cycle (by binding to a site on polymerized microtubules distinct from the Paclitaxel binding site). This may, in turn, lead to the accumulation of M-Op18 at the G2/M stage of the cell cycle. Thus, we next sought to determine whether the Op18 mutation affected spindle formation. Both mutant and sense overexpressers were grown in cell chambers, fixed, and then analyzed by immunofluorescence for either α- or β-tubulin-containing mitotic spindles (Figure 6). Whereas 3/493 mitotic spindles were multipolar (more than two spindle poles) in the S-Op18 population, 14/656 mitotic spindles were multipolar in the M-Op18 population—approximately a 4-fold increase in multipolar spindles in the M-Op18-expressing cells ($p = 0.046$, two-sided Fisher's exact test).

Our results described above suggest that the mutation in Op18 interfered with the degree of phosphorylation of the mutated protein in vivo. As the dephosphorylated form of Op18 has been shown to bind to microtubules and stabilize tubulin

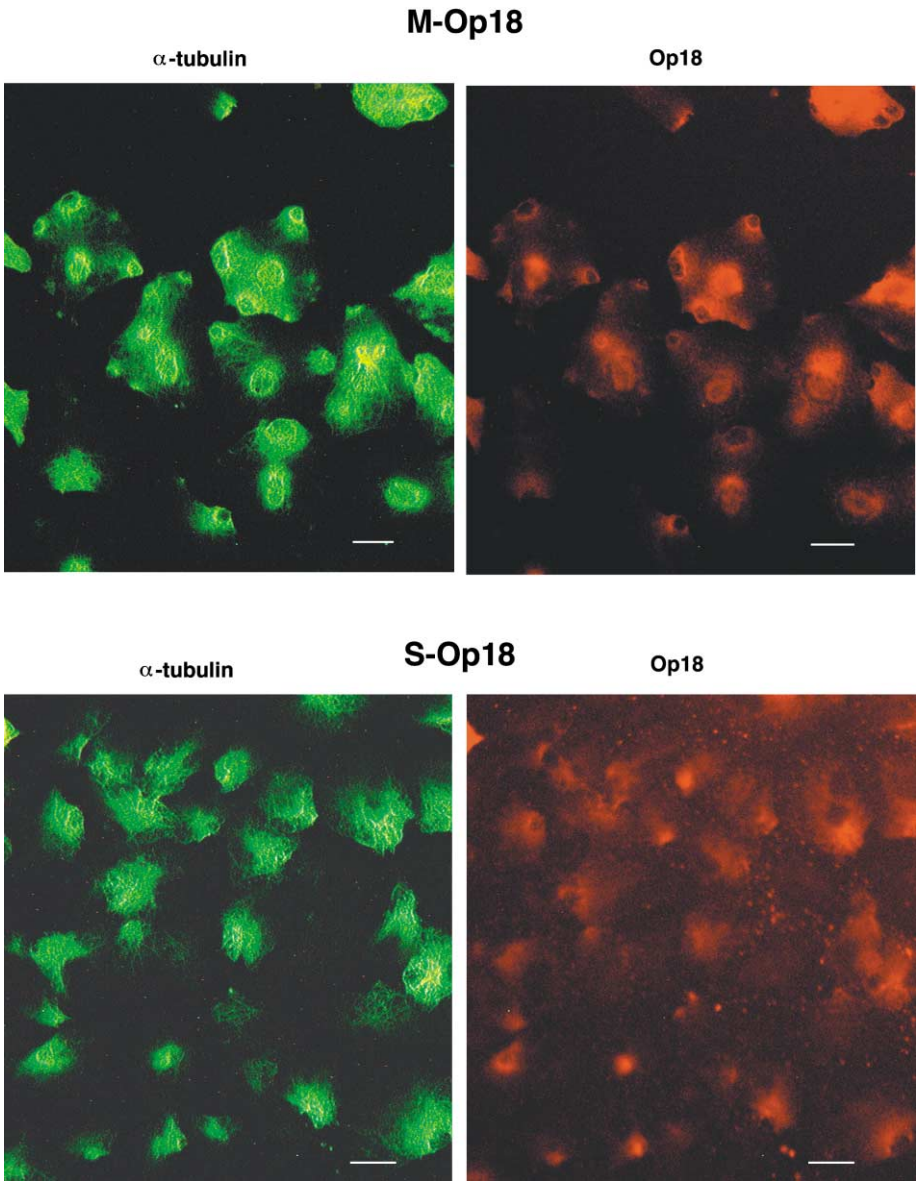

Figure 7. M-Op18 expression results in profound reorganization of microtubule ultrastructure in NIH/3T3 infectants

M-Op18 and S-Op18 infectants were plated and grown at subconfluent levels for 48 hr and then fixed and stained for immunofluorescence with rabbit anti-Op18 antibodies and mouse anti-α-tubulin, as described in Experimental Procedures. Identical fields are shown for both the Op18 antibody and for the anti-α-tubulin antibody. Equivalent results were obtained when an anti-β-tubulin antibody was used instead of the anti-α-tubulin antibody. The experiment has been repeated five times. Bar equals 10 μm.

dimers, we sought to ascertain whether expression of the mutated form of Op18 would lead to increased stabilization of microtubules with associated changes in microtubular ultrastructure as compared to that visualized with S-Op18. Both M-Op18 and S-Op18 cells were plated on chamber slides, then subsequently stained for either α-tubulin, β-tubulin, or γ-tubulin (found in centrosomes) immunofluorescence, in the presence or absence of immuofluorescent staining of Op18. Overall, we observed unusual rings and swirls of both α- and β-tubulin immunoreactivity near the cell periphery in the NIH/3T3 cells expressing M-Op18 (Figure 7). No similar structures were visualized in NIH/3T3 cells expressing S-Op18. Further, we did not find any differences in the numbers of centrosomes or in their subcellular location between M-Op18 and S-Op18 infectants, as visualized by γ-tubulin immunofluorescence (data not shown). The rings and swirls of α- and β-tubulin immunoreactivity colocalized with immunofluorescent staining patterns observed with anti-Op18 antibodies, suggesting that Op18 was associated with these structures. The immunoreactive structures appear to be composed of polymerized tubulin molecules (e.g., microtubules), as brief treatment of M-Op18 cells with the microtubule depolymerizing agent nocodazole caused their complete disappearance (data not shown).

Phosphorylation of M-Op18 is reduced as compared with wild-type Op18

The results described above suggested that expression of the mutated form of Op18 interfered with cell cycle dynamics. Thus, we sought to ascertain the mechanistic reason(s) for the observed changes in cell growth and tumorigenic potential in cells expressing M-Op18. Op18 is one of the major mitotic phosphorylation substrates in a number of different cell types, being phosphorylated on up to four serine residues (namely serine 16, serine 25, serine 38, and serine 63) in response to a myriad of extracellular signals. As the mutated form of Op18 involved an amino acid substitution (glutamine to glutamic acid) at resi-

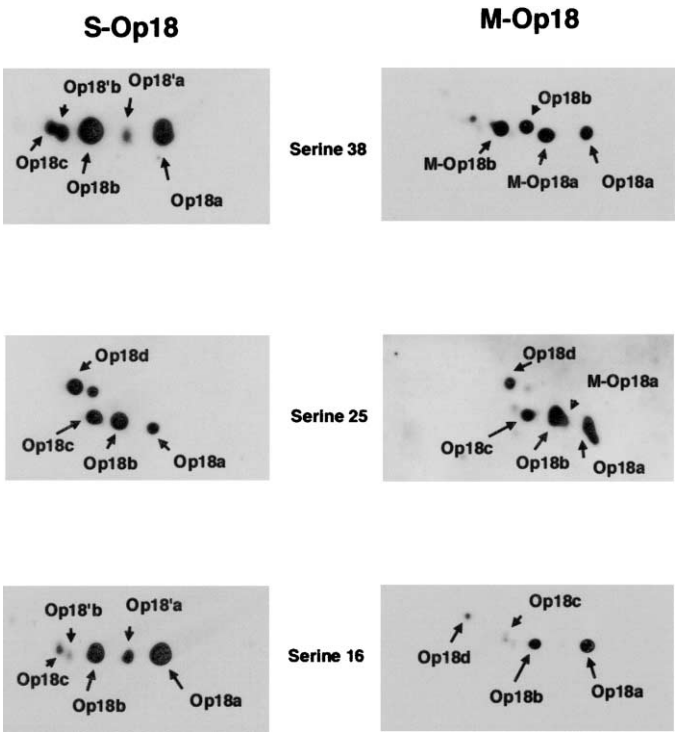

Figure 8. Western blot analysis of phosphorylated Op18 isoforms in NIH/3T3 infectants

Proteins from solubilized NIH/3T3 infectants were separated by 2D PAGE, transferred to PVDF membranes, and hybridized against phosphoserine-specific antibodies, as described in Experimental Procedures. Only the close-up sections framing Op18 protein are shown. Arrows point to a major phosphorylated isoform of Op18 (labeled Op18a), a minor form (Op18'a), which is phosphorylated on one of the four phosphorylatable serine residues, and several minor isoforms, which are phosphorylated on several serine residues (Op18'b, Op18b, c ,and d, respectively). The phosphorylated (on a single serine residue) mutant form of Op18 is indicated as M-Op18a, with its doubly phosphorylated isoform indicated as M-Op18b.

due 18, which ultimately resulted in a full charge (plus to minus) difference immediately adjacent to two key phosphorylation sites, we postulated that the Op18 mutation might have resulted in decreased levels of phosphorylation of the mutant protein as compared to the levels observed with wild-type. In order to evaluate the capacity of all phenotypes of the infected cells to phosphorylate cellular proteins, especially the various forms of Op18, cells were labeled in vivo with ^{32}P for 2 hr. The labeled proteins were resolved by 2D PAGE and imaged by exposure of the dried gels to film. Op18 isoforms previously shown to be phosphorylated (Wang et al., 1993) were identified, and their expression levels were analyzed. Overall, we found that the levels of both the mono- and biphosphorylated forms of M-Op18 were substantially reduced as compared with these phosphorylated forms of wild-type Op18, while the levels of all other cellular phosphoproteins detected remained invariant (data not shown). To further explore which of the phosphorylation sites on the M-Op18 was adversely affected by the mutated phenotype, Western blot analysis of both the M-Op18 and S-Op18 was performed (Figure 8) using site-specific rabbit antibodies to phosphoserine 16, phosphoserine 25, and phosphoserine 38 (an antibody to phosphoserine 63 was unavailable). We found that phosphorylation of serine 38 was largely unaffected by the mutant phenotype as compared with the wild-type phenotype. In marked contrast, however, phosphorylation of serine 25 in M-Op18 was greatly reduced when compared with that observed on wild-type. Additionally, there was no phosphorylation of serine 16 detectable in M-Op18 (although we were able to detect it in S-Op18). This situation might result from the perturbation of the epitope by the glutamine to glutamic acid substitution occurring at serine 18 and may not necessarily reflect the true phosphorylation state of M-Op18 serine 16.

Discussion

We have uncovered in our analysis of Op18 expression in esophageal tumors a $C_{52}\rightarrow G$ mutation in the Op18 coding region, which results in a Q18→E substitution. This is a report of a novel Op18 mutation found in cancer. The Q18→E substitution in Op18 was not detected in normal esophageal and Barrett's tissue from the same patient, indicating it was a somatic mutation that arose in the tumor. Analysis of genomic DNA revealed a similar band intensity of the PCR products representing the mutated and wild-type Op18 gene in the tumor that exhibited only mutant Op18 protein. It is plausible that associated nontumor cells in the tumor sample gave rise to the band representing the wild-type PCR product. Although we cannot exclude the possible alteration in the rate of amplifying wild-type and the mutant Op18 genes, it seems unlikely this would occur for two 489 bp fragments that differ in only one nucleotide. Furthermore, the probability of the same somatic mutation occurring at two alleles is very rare. Thus, the $C_{52}\rightarrow G$ mutation likely occurred at one of the two alleles in the tumor in which it was detected.

Even though only one allele may be mutated, the tumor that expressed mutant Op18 exclusively expressed the mutant. One plausible explanation is that Op18 in the tumor may be monoallelically expressed, specifically from the allele containing the mutated Op18. Another possibility for the lack of wild-type Op18 expression in this tumor is that the region containing the wild-type Op18 gene in the other allele may be deleted. The Op18 gene is located on chromosome 1p36 (Ferrari et al., 1990), and the deletion of this region is commonly observed in cancers including breast and colon carcinomas (Farabegoli et al., 1996; Tanaka et al., 1993). Based on Southern blot analysis using the enzymes that cut within the Op18 gene, however, we did not observe a gross deletion or rearrangement in the genomic DNA from this tumor, as compared to tissues from the other 16 patients studied (data not shown). Another possibility is that expression of the mutated Op18 affects the expression or protein stability of wild-type Op18. However, this is also unlikely based on our results from pulse-chase experiments.

Our data, based on the analysis of 17 esophageal tumors, indicates total loss of wild-type Op18 and the presence of only the mutated form in just one tumor. In the other tumors, we cannot exclude the occurrence of small amounts of mutated Op18. Although we have observed some Op18 that migrates to the same position on 2D gel as the mutant form, such minor forms may represent modifications other than the specific mutation we have observed, since we do not have an antibody that is specific for the mutant form.

The Q18→E mutation introduces a negative charge to Op18 protein, thereby inducing a structural change that may alter its proper interaction with other cellular proteins, most notably

tubulin and various serine/threonine protein kinases (Belmont and Mitchison, 1996; Beretta et al., 1993; Curmi et al., 1994; Luo et al., 1994; Marklund et al., 1993, 1994; Maucuer et al., 1995). By altering the interaction with kinases, phosphorylation of the mutated Op18 may be negatively affected, especially on the phosphorylatable serine residues (S16 and S25) immediately surrounding the site of the mutation. It has been shown that wild-type Op18 exhibits a microtubule-destabilizing activity in vivo (Belmont and Mitchison, 1996), which can be downregulated by phosphorylation on four serine (S16, S25, S38, and S63) residues (Gavet et al., 1998; Horwitz et al., 1997). Increased S16 phosphorylation, in particular, suppressed the microtubule-destabilizing activity of Op18 (Gavet et al., 1998; Melander Gradin et al., 1997). We have demonstrated that overexpression of the Q18→E mutant exhibits reduced overall phosphorylation levels. Although we have not conclusively demonstrated that phosphorylation of S16 is negatively impacted by the Q18→E mutation, we have been unable to detect it with the anti-phosphoserine antibody (even though we can detect phosphorylation on S16 in the wild-type Op18). Decreased phosphorylation on S16 may also significantly impact upon other known biological activities, including impairment of normal spindle formation at mitosis and a blockage of the cell cycle (as demonstrated by overexpression of a nonphosphorylatable (4A) Op18 mutant (Gavet et al., 1998; Larsson et al., 1997; Marklund et al., 1996). We have shown that overexpression of the Q18→E mutant in NIH/3T3 cells results in a 4-fold increase in multipolar spindles and a doubling in the percentage of cells at G2/M by cell cycle analysis as compared to overexpression of the wild-type form of Op18.

In higher eukaryotes, progression through the cell cycle is regulated by cyclin-dependent kinases, with entry into mitosis being controlled by p34-cdc2 (Coleman and Dunphy, 1994). Two of the four Op18 phosphorylatable serines, S25 and S38, are cyclin-dependent kinase consensus phosphorylation sites. Op18 is efficiently phosphorylated in vitro by the activity of p34-cdc2 and p33-cdk2 on both of these sites (Beretta et al., 1993; Brattsand et al., 1994; Marklund et al., 1993). Additionally, expression of an Op18 S25A, S38A dominant-negative mutant has been shown to greatly diminish the level of phosphorylation found at S16 and that this expression was sufficient to cause a G2/M blockage, presumably due to decreased Op18 phosphorylation by cyclin-dependent kinases (Larsson et al., 1995). We have found that, although phosphorylation of S38 was largely unaffected by the mutant phenotype, phosphorylation of S25 in M-Op18 was greatly reduced when compared with that observed on wild-type Op18, and we were unable to detect S16 phosphorylation in the M-Op18-expressing cells. It is conceivable that the Q18→E mutant phenotype we have uncovered is sufficient to reduce the ability of p34-cdc2 to phosphorylate Op18 S25, a phosphorylation site located just seven amino acid residues downstream of the mutation. In turn, this may (directly or indirectly) have had adverse effects on the phosphorylation of S16, located just two amino acid residues upstream of the mutation. This decrease in phosphorylation may ultimately contribute to the observed doubling in M-Op18 cells at G2/M as compared to wild-type overexpressers. An alternative possibility is that the association kinetics between the mutant Op18 and either p34-cdc2 or p33-cdk2 is perturbed compared to that observed with wild-type Op18. Such a change in association constants between M-Op18 and p34-cdc2 might be sufficient to cause the G2/M blockage that we have observed. However, while entry into mitosis is controlled by p34-cdc2, centrosome duplication in vivo has been shown to be dependent upon p33-cdk2 activity (Lacey et al., 1999). It is possible that the kinetics of association between M-Op18 and p33-cdk2 may also be diminished sufficiently during critical portions of the cell cycle. Thus, with the active form of p33-cdk2 not being "sequestered" by Op18, this may favor interactions between p33-cdk2 and other proteins with which it could interact, which in turn could lead to increased numbers of centrosomes, multipolar spindle formation, aneuploidy, and subsequently tumorigenesis.

Recently, Op18 has been shown to accumulate at centrosomes in both HeLa cells and in spindles assembled from *Xenopus* egg extracts (Kuntziger et al., 2001). The polar accumulation observed in *Xenopus* egg extracts supplemented with mutant forms, representing either nonphosphorylatable or hyperphosphorylatable Op18, suggests that centrosomal accumulation of Op18 is independent of phosphorylation state. It has been demonstrated, however, that many other proteins, such as tubulin, nucleophosmin, pericentrin, katanin, and others, are present and/or do accumulate at centrosomes. It is interesting to speculate that Op18 interacts with so-called regulatory proteins in centrosomes, thereby helping to maintain mitotic apparatus fidelity. It is possible that the Q18→E mutant failed to properly interact with one of these proteins, leading to an increase in the number of centrosomes and resulting in multipolar spindle formation. We did not observe changes in the numbers of centrosomes or, for that matter, aneuploidy in the NIH/3T3 cells overexpressing M-Op18 as compared to those expressing S-Op18. However, the M-Op18 cells do express a normal amount of wild-type Op18, possibly sufficient to maintain fidelity in centrosome numbers in the infected NIH/3T3 cells.

Coordination of microtubule dynamics, membrane organization, and DNA synthesis is achieved by a regulatory system responsive to checkpoints at major transitions in the eukaryotic cell cycle. Alterations in the levels and/or functionality of individual protein participants may have profound ramifications for downstream pathways, protein-protein interactions, and cellular homeostasis and might eventually lead to neoplastic changes in the affected cells and tissues. The downstream events leading to tumorigenesis in the M-Op18-expressing cells are presently unclear. We have undertaken an extensive proteomic analysis of the NIH/3T3 cells overexpressing M-Op18 as compared with the wild-type Op18, searching for differences in the expressed protein profiles between these two populations of cells. We have found several differences, including but not limited to vimentin overexpression in the M-Op18 population. While the identity of most of the affected proteins remains to be determined, it is evident that the Op18 mutation we have uncovered has a profound effect on cell homeostasis and points to a potential role for Op18 in abnormal cell proliferation. Additional studies will need to be undertaken to search for Op18 mutations in a variety of cancers and to develop mouse models with various Op18 mutations.

Experimental procedures

Materials

All cell culture reagents, including Dulbecco's modified Eagle's medium (DMEM, containing L-glutamine, sodium pyruvate, and pyridoxine hydrochloride), Dulbecco's phosphate buffered saline (D-PBS), fetal calf serum, penicillin/streptomycin, and Geneticin (G-418) were obtained from GIBCO-

BRL (Grand Island, NY). The hygromycin was purchased from Roche (Indianapolis, IN). The 2-well chamber slides were from Nalge-Nunc (Napierville, IL). The mouse monoclonal anti-α-tubulin, anti-β-tubulin, and anti-γ-tubulin antibodies were purchased from Sigma Chemical Co. (St. Louis, MO). The rabbit anti-Op18 antibodies and the specific anti-Op18 phosphoserine antibodies were a kind gift of Dr. Andre Sobel (INSERM, Paris, France). The pTP2000 bicistronic expression vector and the ϕNX retroviral-producing cell line were a kind gift of Dr. Eric Radany (University of Michigan, Ann Arbor, Michigan). The horseradish peroxidase-conjugated donkey anti-rabbit IgG and the ECL (Enhanced Chemiluminescence) kit were obtained from Amersham (Arlington Heights, IL). The Alexa 594 highly crossadsorbed goat anti-rabbit IgG, the Alexa 488 highly crossadsorbed goat anti-mouse IgG, the DAPI (4′,6-diamidino-2-phenylindole dihydrochloride), and the Paclitaxel (Taxol) were all obtained from Molecular Probes (Eugene, OR). The anti-Cytokeratin AE1/AE3 antibody was obtained from Roche (Indianapolis, IN). The Immobilon-P PVDF (polyvinylidine fluoride) membranes were purchased from Millipore Corp (Bedford, MA). The acrylamide used in the first-dimension electrophoresis, urea, ammonium persulfate, and PDA (piperazine diacrylamide) were all purchased from Bio-Rad (Rockville Centre, NY). The acrylamide used in the second-dimension electrophoresis was purchased from Serva (Crescent Chemical, Hauppauge, NY), and the carrier ampholytes (both pH 4–8 and pH 3.5–10) and NP-40 were both purchased from Gallard/Schlessinger (Carle Place, NY). All other reagents and chemicals were obtained from either Fisher or Sigma and were of the highest purity available.

Cell growth

Both the ϕNX retroviral-producing cell line and the NIH/3T3 cells were cultured at 37°C in a 6% CO_2-humidified incubator in DMEM supplemented with 10% fetal calf serum, 100 U/ml penicillin, and 100 U/ml streptomycin. The cells were passaged weekly upon reaching confluence. Once infected with the retrovirus, each population of NIH/3T3 cells was maintained as above, with the additional presence of either 100 μg/ml hygromycin or 400 μg/ml Geneticin.

Quantitative 2D PAGE and Western blotting

Patients undergoing resection for esophageal cancer by the General Thoracic Surgery Section at The University of Michigan Hospital between 1991 and 1994 were evaluated for inclusion in this study. All patient identifiers were removed. Consent was received from all patients, and the protocol approved by The University of Michigan Institutional Review Board (Medicine). Fresh tumor tissue and nontumor containing normal esophagus and gastric mucosa was obtained from patients with esophageal or gastric cardia tumors. Following excision, the tumor tissue was immediately frozen at –80°C. Only tumors with greater than 70% cellularity were used in this study. Total proteins in tissues and the infected NIH/3T3 cells (described below) were analyzed by 2D PAGE (Strahler et al., 1989). Briefly, proteins were solubilized with lysis buffer, containing 8 M urea, 2% pH 3.5–10 carrier ampholytes, 2% β-mercaptoethanol, 2% Nonidet-P40, and 10 mM PMSF. Isoelectric focusing was carried out for 13,200 volt-hours at room temperature, using pH 4–8 carrier ampholytes. The first-dimension tube gel was loaded onto a cassette containing the second-dimension gel, after equilibration in second-dimension sample buffer (125 mM Tris [pH 6.8], containing 10% glycerol, 2% SDS, 1% dithiothreitol, and bromophenol blue). Separation in the second dimension was performed by electrophoresis in 11%–14% polyacrylamide gradient SDS gels, and the samples were electrophoresed until the dye front reached the opposite end of the gel. Gels were silver-stained and digitized for protein spot quantitation as previously described (Kuick et al., 1987). Radioactivity of phosphoprotein patterns were visualized and quantitated by phosphorimage technology (Johnston et al., 1990). For some gels, the resolved proteins were transferred to an Immobilon-P PVDF membrane. Protein patterns on some membranes were visualized by Coomassie blue staining of the membranes. Unstained membranes prepared for hybridization were incubated with blocking buffer (consisting of Tris buffered saline [TBS] containing 1.8% nonfat dry milk and 0.1% Tween 20) for 2 hr, then washed and incubated with specific primary antibodies diluted in blocking buffer for 1 hr at room temperature. Following three washes with blocking buffer, the membranes were incubated with a horseradish peroxidase-conjugated donkey anti-rabbit IgG antibody (at a 1:1000 dilution) for 1 hr at room temperature. The membranes were washed five times with TBS containing 0.1% Tween 20, once in TBS, briefly incubated in ECL, and exposed to XAR-5 X-ray film. Patterns visualized were directly compared to both the Coomassie blue-stained sister gels, as well as to sister gel silver-stain patterns.

RT-PCR and DNA sequencing

PolyA$^+$ mRNA was isolated from the esophageal tumor of patient #7 using a mRNA isolation kit (Invitrogen Corp., Carlsbad, CA). The purified RNA was reverse-transcribed using AMV reverse transcriptase (New England BioLabs, Beverly, MA) prior to PCR. The Op18s (CCT GTC GCT TGT CTT CTA TTC ACC) and Op18a (GGG ATG GGG AGA AAG TCA GTT C) primers were designed to amplify the Op18 cDNA containing the coding region spanning from nucleotide residue 80 to 585 (Zhu et al., 1989). Amplification was performed with 35 cycles consisting of denaturation at 94°C for 1 min, annealing at 68°C for 1 min, and extension at 72°C for 1 min. The PCR products were resolved by gel electrophoresis, directly purified from the agarose gel, and then subjected to fluorescence DNA sequencing with the ABI 373A Sequencer at the Core Facility of the University of Michigan.

Screening the C_{155}→G mutation in the Op18 gene

Genomic DNA was purified from the esophageal tumors and normal tissues of seven patients using the method described previously (Thoraval et al., 1996). The Op18-3761 (GGT GAA AGA ACT GGA GAA GCG TG) and Op18-4249 primers (TGG TTT AAG ATA GAC CAG GGC TTG) were selected to amplify a 489 bp fragment containing the site of mutation in the Op18 gene. PCR was performed with 35 cycles consisting of denaturation for 1 min at 94°C, annealing for 1 min at 60°C, and extension for 1 min at 72°C. The amplified products were digested with ScrF1 restriction enzyme and subsequently analyzed by gel electrophoresis. The DNA fragments in the gel were stained with ethidium bromide for visualization.

Generation of NIH/3T3 infectants that expressed the mutated Op18 (M-Op18)

The mutant Op18 cDNA obtained by RT-PCR from the esophageal tumor of patient #7 was cloned into the pCRII vector (Invitrogen). The resultant pCRII-Op18mt plasmid was subjected to a second round of DNA sequencing prior to further studies. Additionally, a 555 bp wild-type Op18 cDNA was also subcloned into the pCRII vector. Both cDNAs were subsequently cloned into the pTP2000 bicistronic expression vector. The resulting constructs were used to transfect the ϕNX retroviral-producing cell line. Briefly, ϕNX cells were grown to approximately 70% confluence. Fifty micrograms of each pTP2000 construct (vector only, sense wild-type, antisense wild-type, and mutant) was introduced into the ϕNX cells by calcium phosphate transfection. The resultant supernatants were harvested 48 hr after transfection and subjected to centrifugation at 1000 × g for 15 min at 4°C, followed by centrifugation at 3600 × g for 15 min at 4°C, then frozen at −80°C until use. The NIH/3T3 cells were plated at 40%–50% confluence and then exposed to the retrovirus-containing supernatants for 4 hr in the presence of 4 μg/ml hexadimethrine bromide (Sigma). Following a brief wash, the cells were incubated for 48 hr in DMEM containing 10% fetal calf serum and antibiotics. Infectants were selected with hygromycin at an optimal concentration of 300 μg/ml. The Op18 protein isoforms of each infectant were evaluated by 2D PAGE.

Soft agar transformation

To analyze the ability of the Op18 transfectants to exhibit anchorage independent growth, cells were assayed for their ability to form colonies in soft agar. 1×10^4 cells of each infectant were plated in 0.35% Noble agar over a cushion of 0.7% Noble agar, in quintuplicate. Cells were fed full-growth medium (90% DMEM, 10% FCS containing antibiotics and G418 [400 μg/ml]) and assayed for colony formation at 35 days using an inverted microscope.

Cell cycle analysis

Cell cycle analysis was performed at The University of Michigan Cancer Center Flow Cytometry Core Facility according to standard procedure. Briefly, the NIH/3T3 infectants were plated and grown at subconfluent levels for 48 hr in 100 cm^2 tissue culture dishes and then treated with increasing concentrations of Paclitaxel for an additional 24 hr. All treatment groups were analyzed by flow cytometry for cell cycle distribution at 72 hr following plating. Cells were resuspended by brief trypsinization and washed in D-PBS. 1×10^6 cells per sample were resuspended in 0.5 ml D-PBS, then fixed by

addition of 0.5 ml cold 100% ethanol (added dropwise while vortexing). Cells were incubated on ice for 20 min, then pelleted by centrifugation at 1000 × g for 5 min. The tubes were inverted in order to remove ethanol. Following addition of 0.5 ml of propidium iodide-RNase solution (50 μg/ml propidium iodide, 100 μg/ml RNase [Type 1-A] in D-PBS) and 50 μl of trout red cell nuclei (an internal control for peak positioning and ploidy; Riese Enterprises, Grass Valley, CA), the samples were mixed and incubated in the dark for 20 min. 1×10^4 cells per sample were analyzed by Flow Cytometry using the Coulter Elite Software Package (Beckman-Coulter, Miami, FL) for analysis of DNA content (propidium iodide labeling of nuclei). The Multicycle Software Package (Phoenix Flow Systems, San Diego, CA) was used to determine the percentage of cells in each stage of the cell cycle.

Immunofluorescence

The NIH/3T3 infectants were grown in 2-well chamber slides for 48 hr, then fixed in 2% formaldehyde, freshly prepared from paraformaldehyde. The fixed cells were washed briefly in D-PBS (Dulbecco's Phosphate Buffered Saline) and permeabilized by addition of 0.2% Tween 20 (in D-PBS). Aldehyde groups resulting from fixation were quenched in 50 mM glycine (in D-PBS), after which the fixed monolayers were washed three times in D-PBS (containing 1 mg/ml BSA). Each chamber was incubated with 0.5 ml of the appropriate primary antibody diluted as indicated in D-PBS (containing 1 mg/ml BSA) for 45 min at room temperature. The monolayers were washed in D-PBS (containing 1 mg/ml BSA), then incubated with 0.5 ml D-PBS (containing 1 mg/ml BSA) containing either 20 μg/ml highly crossadsorbed Alexa-594-conjugated goat anti-rabbit IgG (used when rabbit serum was used as the primary antibody) or 20 μg/ml highly crossadsorbed Alexa-488-conjugated goat anti-mouse IgG (used when a mouse monoclonal antibody was used as the primary antibody). The stained monolayers were washed three times in D-PBS (containing 1 mg/ml BSA) and three times in D-PBS, after which a glass coverslip was mounted on the monolayers in GEL/MOUNT (Biomeda Corp., Foster City, CA). Fluorescent images were visualized through a Leitz Orthoplan Microscope and processed through a Sony Digital Imaging Camera.

Acknowledgments

The authors would like to thank Dr. Andre Sobel (INSERM, Paris, France) for the kind gift of the rabbit anti-Op18 antibody, as well as for the Op18 phosphoserine-specific antibodies. We thank Dr. Eric Radany (Department of Radiation Oncology, University of Michigan, Ann Arbor, Michigan) for the kind gift of the pTP2000 expression vector and for the ϕNX cells. We thank Dr. Eric Sheldon (University of Michigan) for helpful discussions. We are grateful to Dr. Latha Prasannan and Chris Edwards for technical assistance with the fluorescence microscopy, to Eric Puravs for assistance with figure preparation, and to Donna Gauss for assistance with the manuscript. This study was funded, in part, by the NCI Director's Challenge grant CA84953 (to S.M.H.) and the National Institutes of Health grant CA71606 (to D.G.B.).

Received: May 23, 2002
Revised: August 21, 2002

References

Belmont, L.D., and Mitchison, T.J. (1996). Identification of a protein that interacts with tubulin dimers and increases the catastrophe rate of microtubules. Cell *84*, 623–631.

Beretta, L., Dobránsky, T., and Sobel, A. (1993). Multiple phosphorylation of stathmin. Identification of four sites phosphorylated in intact cells and in vitro by cyclic AMP-dependent protein kinase and p34cdc2. J. Biol. Chem. *268*, 20076–20084.

Brattsand, G., Roos, G., Marklund, U., Ueda, H., Landberg, G., Nanberg, E., Sideras, P., and Gullberg, M. (1993). Quantitative analysis of the expression and regulation of an activation-regulated phosphoprotein (oncoprotein 18) in normal and neoplastic cells. Leukemia *7*, 569–579.

Brattsand, G., Marklund, U., Nylander, K., Roos, G., and Gullberg, M. (1994). Cell cycle regulated phosphorylation of oncoprotein 18 on Ser16, Ser25, and Ser38. Eur. J. Biochem. *20*, 359–368.

Coleman, T.R., and Dunphy, W.G. (1994). Cdc2 regulatory factors. Curr. Opin. Cell Biol. *6*, 877–882.

Cooper, H.L., McDuffie, E., and Braverman, R. (1989). Human peripheral lymphocyte growth regulation and response to phorbol esters is linked to synthesis and phosphorylation of the cytosolic protein, prosolin. J. Immunol. *143*, 956–963.

Curmi, P.A., Maucuer, A., Asselin, S., Lecourtois, M., Chaffotte, A., Schmitter, J.M., and Sobel, A. (1994). Molecular characterization of human stathmin expressed in *Escherichia coli*: site-directed mutagenesis of two phosphorylatable serines (Ser-25 and Ser-63). Biochem. J. *300*, 331–338.

Curmi, P.A., Nogues, C., Lachkar, S., Carelle, N., Gonthier, M.P., Sobel, A., Lidereau, R., and Bieche, I. (2000). Overexpression of stathmin in breast carcinomas points out to highly proliferative tumours. Br. J. Cancer *82*, 42–50.

Farabegoli, F., Ceccarelli, C., Santini, D., Trere, D., Baldini, N., Taffurelli, M., and Derenzini, M. (1996). Chromosome 1 aneusomy with 1p36 underrepresentation is related to histologic grade, DNA aneuploidy, high c-erb B-2 and loss of bcl-2 expression in ductal breast carcinoma. Int. J. Cancer *69*, 381–385.

Ferrari, A.C., Seuanez, H.M., Hanash, S.M., and Atweh, G.F. (1990). A gene that encodes for a leukemia-associated phosphoprotein (p18) maps to chromosome band 1p35-36.1. Genes Chromosomes Cancer *2*, 125–129.

Gavet, O., Ozon, S., Manceau, V., Lawler, S., Curmi, P., and Sobel, A. (1998). The stathmin phosphoprotein family: intracellular localization and effects on the microtubule network. J. Cell Sci. *111*, 3333–3346.

Hailat, N., Strahler, J., Melhem, R., Zhu, X.X., Brodeur, G., Seeger, R.C., Reynolds, C.P., and Hanash, S.M. (1990). N-*myc* gene amplification in neuroblastoma is associated with altered phosphorylation of a proliferation related polypeptide (Op18). Oncogene *5*, 1615–1618.

Hanash, S.M., Strahler, J.R., Kuick, R., Chu, E.H.Y., and Nichols, D. (1988). Identification of a polypeptide associated with the malignant phenotype in acute leukemia. J. Biol. Chem. *263*, 12813–12815.

Horwitz, S.B., Shen, H.J., He, L., Dittmar, P., Neef, R., Chen, J., and Schubart, U.K. (1997). The microtubule-destabilizing activity of metablastin (p19) is controlled by phosphorylation. J. Biol. Chem. *272*, 8129–8132.

Johnston, R.F., Pickett, S.C., and Barker, D.L. (1990). Autoradiography using storage phosphor technology. Electrophoresis *11*, 355–360.

Jourdain, L., Curmi, P., Sobel, A., Pantaloni, D., and Carlier, M.F. (1997). Stathmin: a tubulin-sequencing protein which forms a ternary T2S complex with two tubulin molecules. Biochemistry *36*, 10817–10821.

Kuick, R., Hanash, S.M., Chu, E.H.Y., and Strahler, J.R. (1987). A comparison of some adjustment techniques for use with quantitative spot data. Electrophoresis *8*, 199–204.

Kuntziger, T., Gavet, O., Sobel, A., and Bornens, M. (2001). Differential effect of two stathmin/Op18 phosphorylation mutants on xenopus embryo development. J. Biol. Chem. *276*, 22979–22984.

Lacey, K.R., Jackson, P.K., and Stearns, T. (1999). Cyclin-dependent kinase control of centrosome duplication. Proc. Natl. Acad. Sci. USA *96*, 2817–2822.

Larsson, N., Melander, H., Marklund, U., Osterman, Ö., and Gullberg, M. (1995). G2/M transition requires multisite phosphorylation of oncoprotein 18 by two distinct protein kinase systems. J. Biol. Chem. *23*, 14175–14183.

Larsson, N., Marklund, U., Gradin, H.M., Brattsand, G., and Gullberg, M. (1997). Control of microtubule dynamics by oncoprotein 18: dissection of the regulatory role of multisite phosphorylation during mitosis. Mol. Cell. Biochem. *17*, 5530–5539.

Luo, X.-N., Mookerjee, B., Ferrari, A., Mistry, S., and Atweh, G. (1994). Regulation of phosphoprotein p18 in leukemic cells. Cell cycle regulated phosphorylation by p34cdc2 kinase. The J. Biol. Chem. *269*, 10312–10318.

Marklund, U., Brattsand, G., Shingler, V., and Gullberg, M. (1993). Serine 25 of oncoprotein 18 is a major cytosolic target for the mitogen-activated protein kinase. J. Biol. Chem. *268*, 15039–15047.

Marklund, U., Larsson, N., Brattsand, G., Osterman, O., Chatila, T.A., and Gullberg, M. (1994). Serine 16 of oncoprotein 18 is a major cytosolic target for the Ca2+/calmodulin-dependent kinase-Gr. Eur. J. Biochem. *225*, 53–60.

Marklund, U., Larsson, N., Gradin, H.M., Brattsand, G., and Gullberg, M. (1996). Oncoprotein 18 is a phosphorylation-responsive regulator of microtubule dynamics. EMBO J. *15*, 5290–5298.

Maucuer, A., Camonis, J.H., and Sobel, A. (1995). Stathmin interaction with a putative kinase and coiled-coil-forming protein domains. Proc. Natl. Acad. Sci. USA *92*, 3100–3104.

Melander Gradin, H., Marklund, U., Larsson, N., Chatila, T.A., and Gullberg, M. (1997). Regulation of microtubule dynamics by Ca2+/calmodulin-dependent kinase IV/Gr-dependent phosphorylation of oncoprotein 18. Mol. Cell. Biol. *17*, 3459–3467.

Melhem, R.F., Zhu, X.X., Hailat, N., Strahler, J., and Hanash, S.M. (1991). Characterization of the gene for a proliferation related phosphoprotein (Op18) expressed in high amounts in acute leukemia. J. Biol. Chem. *266*, 17747–17753.

Roos, G., Brattsand, G., Landberg, G., Marklund, U., and Gullberg, M. (1993). Expression of oncoprotein 18 in human leukemias and lymphomas. Leukemia *7*, 1538–1546.

Rowlands, D.C., Williams, A., Jones, N.A., Guest, S.S., Reynolds, G.M., Barber, P.C., and Brown, G. (1995). Stathmin expression is a feature of proliferating cells of most, if not all, cell lineages. Lab. Invest. *72*, 100–113.

Sobel, A. (1991). Stathmin: a relay phosphoprotein for multiple signal transduction? Trends Biochem. Sci. *16*, 301–305.

Strahler, J.R., Kuick, R., and Hanash, S.M. (1989). Two-dimensional polyacrylamide gel electrophoresis of proteins. In Protein Structure: A Practical Approach, T. Creighton, ed. (Oxford: IRL Press Ltd.), pp. 65–92.

Strahler, J.R., Hailat, N., Lamb, B.J., Rogers, K.P., Underhill, J.A., Melhem, R.F., Keim, D.R., Zhu, X.-X., Kuick, R.D., Fox, D.A., and Hanash, S.M. (1992a). Activation of resting peripheral blood lymphocytes through the T cell receptor induces rapid phosphorylation of Op18. J. Immunol. *149*, 1191–1198.

Strahler, J.R., Lamb, B.J., Ungar, D.R., Fox, D.A., and Hanash, S.M. (1992b). Cell cycle progression is associated with distinct patterns of phosphorylation of Op18. Biochem. Biophys. Res. Commun. *185*, 197–203.

Tanaka, K., Tanoshita, R., Konishi, M., Oshimura, M., Maeda, Y., Mori, T., and Miyaki, M. (1993). Suppression of tumourigenicity in human colon carcinoma cells by introduction of normal chromosome 1p36 region. Oncogene *8*, 2253–2258.

Thoraval, D., Asakawa, J., Kodaira, M., Chang, C., Radany, E., Kuick, R., Lamb, B., Richardson, B., Neel, J.V., Glover, T., and Hanash, S.M. (1996). A methylated human 9-kb repetitive sequence on acrocentric chromosomes is homologous to a subtelomeric repeat in chimpanzee. Proc. Natl. Acad. Sci. USA *93*, 4442–4447.

Wang, Y.K., Liao, P.-C., Allison, J., Gage, D.A., Andrews, P.C., Lubman, D.M., Hanash, S.M., and Strahler, J.R. (1993). Phorbol 12-myristate 13-acetate-induced phosphorylation of Op18 in Jurkat T cells. The J. Biol. Chem. *268*, 14269–14277.

Zhu, X.X., Kozarsky, K., Strahler, J.R., Eckerskorn, C., Lottspeich, F., Melhem, R., Lowe, J., Fox, D.A., Hanash, S.M., and Atweh, G.F. (1989). Molecular cloning of a novel human leukemia associated gene: evidence of conservation in animal species. J. Biol. Chem. *264*, 14556–14560.